

## Confined Catalysis

 How to cite: *Angew. Chem. Int. Ed.* **2023**, *62*, e202208693

International Edition: doi.org/10.1002/anie.202208693

German Edition: doi.org/10.1002/ange.202208693

# Maximum Impact of Ionic Strength on Acid-Catalyzed Reaction Rates Induced by a Zeolite Microporous Environment

Qiang Liu, Niklas Pfriem, Guanhua Cheng, Eszter Baráth, Yue Liu,\* and Johannes A. Lercher\*

**Abstract:** The intracrystalline ionic environment in microporous zeolite can remarkably modify the excess chemical potential of adsorbed reactants and transition states, thereby influencing the catalytic turnover rates. However, a limit of the rate enhancement for aqueous-phase dehydration of alcohols appears to exist for zeolites with high ionic strength. The origin of such limitation has been hypothesized to be caused by the spatial constraints in the pores via, e.g., size exclusion effects. It is demonstrated here that the increase in turnover rate as well as the formation of a maximum and the rate drop are intrinsic consequences of the increasingly dense ionic environment in zeolite. The molecularly sized confines of zeolite create a unique ionic environment that monotonically favors the formation of alcohol-hydronium ion complexes in the micropores. The zeolite microporous environment determines the kinetics of catalytic steps and tailors the impact of ionic strength on catalytic rates.

(H<sub>2</sub>O), zeolitic Brønsted acid sites (BAS), i.e., the acidic bridging hydroxyl groups of zeolite frameworks form hydrated hydronium ions (H<sup>+</sup>(H<sub>2</sub>O)<sub>n</sub>).<sup>[2]</sup> The composition of these intraporous hydronium ion clusters was quantified to be H<sup>+</sup>(H<sub>2</sub>O)<sub>7–8</sub> for the example of proton-exchanged Zeolite Socony Mobil-5 (H-ZSM-5) zeolite through a combination of adsorption of water and aqueous-phase organic substrates.<sup>[2e]</sup> The zeolite-confined nano-environments play important roles in hydronium ion-catalyzed reactions, such as alcohol dehydration<sup>[3]</sup> and phenol alkylation in water.<sup>[4]</sup> The confinement of zeolite pores enables the association of a larger fraction of alcohol molecules with hydronium ions in comparison with that in homogeneous acid solutions, and minimizes the free energies of activation, in turn potentially enhancing hydronium ion-catalyzed reaction rates.<sup>[5]</sup>

The variations in the concentration of hydronium ions in nanoscopic confinements alter the adsorption of reactants, and (de)stabilize surface intermediates and transition states for the catalytic reactions in the zeolite micropores.<sup>[2e,6]</sup> We have shown that the specific interactions between the confined hydronium ions and adsorbed reactants in zeolite induce thermodynamic non-idealities to a catalytic system.<sup>[6]</sup> The turnover rates for intramolecular dehydration of cyclohexanol (CyOH) in water initially increase with the local ionic strength in a micropore, but decrease at higher ionic strength, thus, giving rise to a limitation to the enhancement of catalytic dehydration rates. The local ionic environments with moderate-to-high ionic strength alter the excess chemical potentials (i.e., excess free energies) of adsorbed uncharged reactants and positively charged transition states, which initially increase the reaction rates. The rates drop at higher ionic strength as a consequence of increasing excess chemical potentials of the charged transition states, which in turn raises the activation Gibbs free energies.

Except for the corresponding lattice base site at the aluminum oxygen tetrahedron interacting with the H<sup>+</sup>(H<sub>2</sub>O)<sub>n</sub>, the other micropore space are saturated with substrate molecules in the process of aqueous-phase CyOH dehydration. This leads typically to zeroth-order kinetic dependences in the reacting CyOH concentration.<sup>[3,5,6]</sup> It has been observed in zeolite H-MFI that the adsorption capability (and strength) for CyOH from an aqueous phase decrease with increasing concentration of H<sup>+</sup>(H<sub>2</sub>O)<sub>n</sub> in zeolite pores.<sup>[2e]</sup> In H-MFI pores, the presence of higher concentration of H<sup>+</sup>(H<sub>2</sub>O)<sub>n</sub> decreases the void space between the neighboring hydronium ion clusters, becoming eventually smaller than the van der Waals volume (V<sub>vdw</sub>) of CyOH molecule. This leads to limited adsorption of CyOH

## Introduction

Catalytic reactions on microporous zeolites can be enhanced by tailoring of the nanoscopic environment.<sup>[1]</sup> In liquid water

[\*] Dr. Q. Liu, N. Pfriem, Dr. G. Cheng, Dr. E. Baráth, Prof. Y. Liu, Prof. J. A. Lercher  
 Department of Chemistry and Catalysis Research Center, Technical University of Munich  
 Lichtenbergstrasse 4, 85747 Garching (Germany)  
 E-mail: johannes.lercher@ch.tum.de

Prof. Y. Liu  
 Shanghai Key Laboratory of Green Chemistry and Chemical Processes, School of Chemistry and Molecular Engineering, East China Normal University  
 200062 Shanghai (P. R. China)  
 E-mail: liuyue@chem.ecnu.edu.cn

Prof. J. A. Lercher  
 Institute for Integrated Catalysis, Pacific Northwest National Laboratory  
 P.O. Box 999, Richland, WA 99352 (USA)

© 2022 The Authors. Angewandte Chemie International Edition published by Wiley-VCH GmbH. This is an open access article under the terms of the Creative Commons Attribution Non-Commercial NoDerivs License, which permits use and distribution in any medium, provided the original work is properly cited, the use is non-commercial and no modifications or adaptations are made.

in the pores. This size (volume) exclusion effect has been attributed to the marked reduction in catalytic dehydration turnover rates.<sup>[6,7]</sup> However, it is still unclear whether the production of catalytic rates are caused by these limitations (more  $\text{H}^+(\text{H}_2\text{O})_n$  are present than reacting molecules) or whether the decrease in rate and the lower fraction of reacting molecules in the pores are parallel phenomena caused by changes in the thermodynamic states along the reaction path. To address this question we have decided to study the kinetics under conditions not limited by the maximum uptake of reactive substrates, under conditions leading to a first-order dependence on the substrate chemical potential.

We quantitatively investigate the aqueous-phase CyOH dehydration reaction at low coverages of CyOH to conclusively exclude the influence of limitations in the uptake of the reacting alcohols. Thermochemical and kinetic measurements are used to describe, how the confined ionic environment intrinsically facilitates the accommodation of reaction intermediates and the enthalpic stabilization of charged transition states within zeolite micropores to maximize the alcohol dehydration turnover rates. The position of the maximum turnover rate was observed to be independent of the sorbed state of substrate molecules and reflects the optimal formation of alcohol-hydronium ion interactions and charged transition states.

## Results and Discussion

### Reaction order as a function of CyOH concentration on H-MFI (Si/Al 45)

As outlined above, in aqueous phase structural BAS are transformed to  $\text{H}^+(\text{H}_2\text{O})_n$  and serve as active sites for the catalytic dehydration of CyOH.<sup>[2d,f,5b]</sup> The dehydration of CyOH to cyclohexene on Brønsted acidic zeolite proceeds in the sequence of the formation of associated alcohol-hydronium ion complexes, the protonation of the OH group, accompanied with the stepwise cleavage of C–O bond to carbenium ion intermediate and the deprotonation step to generate the cyclohexene product (Supporting Information, Scheme S1). Previous contributions focused on the aqueous-phase CyOH dehydration in the zeroth-order kinetic regimes catalyzed by microporous zeolites with the starting CyOH concentration ( $[\text{CyOH}] > 100$  mM (millimole per liter)).<sup>[5,6]</sup> Density functional theory modeling and isotope experiments showed that the E1 character involving  $\text{C}_\beta\text{--H}$  bond cleavage as the kinetically relevant step is the more plausible mechanism for the elimination of water.<sup>[5]</sup> A rate expression [Eq. (1)], details of the derivation are shown in the Supporting Information Note S1) derived from transition state theory describes the kinetic dependence of turnover rates on the rate constant  $k_{z,d}$  and the association degree of CyOH with hydronium ions,  $\theta_{z,a}$  [Eq. (2)]:

$$\frac{r}{[\text{H}_3\text{O}^+]_0} = k_{z,d}\theta_{z,a} \quad (1)$$

$$\theta_{z,a} = \frac{K_{L,a} \frac{[\text{CyOH}]_{\text{aq}}}{[\text{H}_2\text{O}]_l}}{1 + K_{L,a} \frac{[\text{CyOH}]_{\text{aq}}}{[\text{H}_2\text{O}]_l}} \quad (2)$$

Here,  $[\text{H}_3\text{O}^+]_0$  is the concentration of hydronium ions,  $K_{L,a}$  represents the equilibrium constant for the association of alcohol-hydronium ion within zeolite pores. Then, the apparent reaction order of CyOH ( $n$ ) is formulated in Equation (3), in particular, as a function of the fractional coverage or the association degree of CyOH with the hydronium ions ( $\theta_{z,a}$ ) (details of the derivation are presented in the Supporting Information Note S1):

$$n = \frac{\partial \ln(r)}{\partial \ln([\text{CyOH}]_{\text{aq}})} = \frac{1}{1 + K_{L,a} \frac{[\text{CyOH}]_{\text{aq}}}{[\text{H}_2\text{O}]_l}} = 1 - \theta_{z,a} \quad (3)$$

The rate of CyOH dehydration over H-MFI 45 (Si/Al 45) as a function of  $[\text{CyOH}]$  in the range of 0.3–100 mM are compiled in Figure 1. The reaction rates of CyOH dehydration in an aqueous phase decreased with the decrease of  $[\text{CyOH}]$  at temperatures of 393 to 413 K, and concurrently, the reaction order increased gradually and approached a first-order kinetic regime ( $1.0 \pm 0.15$  of reaction order) at  $[\text{CyOH}]$  below 1 mM. The increase in the reaction order with respect to the  $[\text{CyOH}]$  decrease is associated to a lower coverage of CyOH molecules. Mass transfer effects in this reaction were assessed by the Weisz-Prater criterion,<sup>[8]</sup> and the results showed an absence of mass transfer limitation (Detail of the calculations see from the Supporting Information Note S2). Therefore, the measured reaction rates are considered to be the intrinsic turnover rates of hydronium ion-catalyzed dehydration of CyOH in the zeolite micropores.

The turnover frequencies (TOFs) measured at  $[\text{CyOH}] = 0.7$  mM by normalizing the reaction rates to the total BAS concentration of H-MFI 45 are 4–6 times lower than those

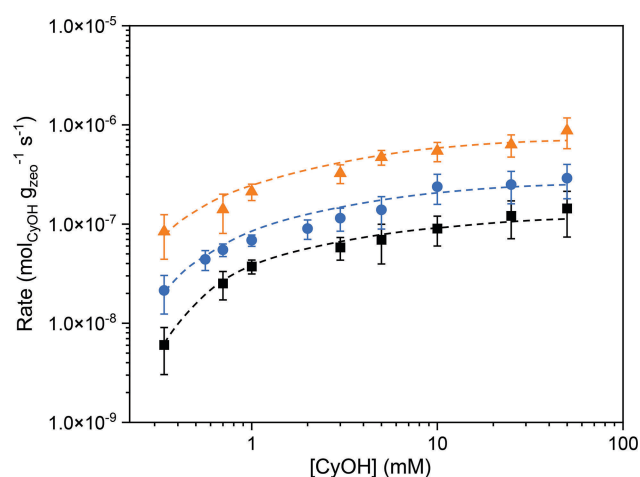


**Figure 1.** Cyclohexanol dehydration rates measured on H-MFI 45 as a function of the concentrations of cyclohexanol in the aqueous phase at 393 K (squares), 403 K (circles), and 413 K (triangles). Dashed lines are to guide the eye.

in the case of zeroth-order kinetic regimes. It is important to note that the turnover rates and TOFs for the CyOH dehydration on H-MFI 45 zeolite are more than two orders of magnitude higher than those measured for unconfined hydronium ions in homogeneous phosphoric acid ( $\text{H}_3\text{PO}_4$ ) solution when both a low and a high concentration of CyOH were applied (Supporting Information, Figure S1). The nanoscopic environment of H-MFI zeolite induces a lower activation free energy (Supporting Information, Table S1), which indicates that the catalytic activity gain from the confinement effects of zeolite is still remarkable although the reaction proceeds in the first-order kinetic regimes. The apparent activation energy for the catalytic dehydration of CyOH with first-order kinetic was  $118 \pm 4 \text{ kJ mol}^{-1}$ , which is about  $24 \pm 6 \text{ kJ mol}^{-1}$  lower than that determined from zeroth-order kinetic regime. The value is in reasonable agreement with the adsorption heat ( $24\text{--}30 \text{ kJ mol}^{-1}$ ) of CyOH on H-MFI zeolites in aqueous phase.<sup>[2e,5b]</sup>

The aqueous-phase adsorption properties of CyOH in zeolite H-MFI 45 pores were evaluated in detail. In the work of Shi et al.,<sup>[5b]</sup> the adsorption equilibrium ( $K_{\text{ads}}^\circ$ ) and saturation uptake ( $q_{\text{max}}$ ) for H-MFI 45 were determined from the Langmuir-type isotherms at room temperature with the values of 304 (dimensionless) and  $0.61 \text{ mmol g}^{-1}$ , respectively (Supporting Information, Table S2). The uptake of CyOH in H-MFI 45 from the aqueous solution with the starting [CyOH] of  $0.7 \text{ mM}$  is  $0.056 \text{ mmol g}^{-1}$ , corresponding to 0.092 of fractional coverage ( $\theta$ ) in the micropore, which is far away from the saturated adsorption. The  $q_{\text{max}}$  value becomes lower due to the density increase of CyOH in zeolite pore at high temperatures.<sup>[9]</sup>  $K_{\text{ads}}^\circ$  was extrapolated to the reaction temperatures with the values of 17 (393 K) and 8.5 (413 K). H-MFI 45 zeolite pore contains  $\approx 0.3$  CyOH molecule per unit cell at [CyOH] of  $0.7 \text{ mM}$  under the temperatures of 393 to 413 K, whereas 1.8–2 per unit cell was estimated for the hydrated hydronium ions (i.e.,  $\text{H}^+(\text{H}_2\text{O})_n$ ).

Note that the nature of hydronium ions confined within H-MFI zeolite pores has been verified independent on the identity of adsorbates (Figure S2–S5, see details from the alcohol adsorption on zeolites from gas phase and from aqueous phase in the Supporting Information) and the temperature as applied.<sup>[6]</sup> In addition, in zeolite pores organic molecules tend to adsorb on the hydrophobic sites, whereas the residual space (i.e., the hydrophilic space) allows the accessibility to the hydronium ions regardless of the saturation state of the pores (Supporting Information, Scheme S2).<sup>[10]</sup> A lower fraction of associated CyOH and  $\text{H}^+(\text{H}_2\text{O})_n$  is, therefore, concluded to exist for the H-MFI zeolite when approaching a first-order kinetic regime (with the low coverage of the substrate molecule). Thus, we conclude that the significantly reduced coverage of CyOH in the pores at first-order reaction is largely responsible for the decreased turnover rates of the aqueous-phase dehydration catalyzed by H-MFI 45 compared to the counterpart at zeroth-order reaction.

The reaction mechanism for aqueous-phase CyOH dehydration with much lower coverage of CyOH on zeolite was studied by measuring the kinetic H/D isotope effects

(KIE). The dehydration reactions of  $\text{C}_6\text{H}_{11}\text{OH}$  and  $\text{C}_6\text{D}_{11}\text{OD}$  were performed at the concentration of  $1 \text{ mM}$  (within the first-order kinetic regime) on H-MFI 45 zeolite at 403 K. Catalytic results showed a turnover rate of  $5.8 \times 10^{-5} \text{ s}^{-1}$  for  $\text{C}_6\text{D}_{11}\text{OD}$  and  $1.9 \times 10^{-4} \text{ s}^{-1}$  for  $\text{C}_6\text{H}_{11}\text{OH}$  (Supporting Information, Table S3), giving a KIE value of  $3.3 \pm 0.5$ , which is in good agreement with those obtained for the zeroth-order kinetic regimes over H-MFI, H-BEA zeolites and also with those from first-order kinetics catalyzed by homogeneous acidic  $\text{H}_3\text{PO}_4$  catalyst.<sup>[5b]</sup> This result indicates that a C–H (D) bond cleavage also in this case is the kinetically relevant step, which can be related to the rate-limiting step in the E1 mechanism for aqueous-phase dehydration of alcohols on zeolites.<sup>[3c,5]</sup>

### **Zeolite-catalyzed dehydration of CyOH within varying ionic environments**

To expand the discussion, a series of H-MFI zeolites with different Si/Al ratios (12, 32, 90, 200) was studied. Chemical and physical properties of all the H-MFI samples including the acidic site concentration and micropore volume are summarized in Table S4 (Supporting Information). For these zeolites, the higher the Si/Al ratio gets, the lower the BAS concentration becomes. No clear correlation between the micropore volume and the Si/Al ratios was observed, suggesting that this depends solidly on synthetic parameters. The ionic strength ( $I$ ), determined by normalizing the BAS concentration to micropore volume, monotonically increased with the concentration of BAS (or  $\text{H}^+(\text{H}_2\text{O})_n$ ) in H-MFI pores. Changes in the BAS concentration from  $0.09 \text{ mmol g}^{-1}$  on H-MFI 200 to  $1.15 \text{ mmol g}^{-1}$  on H-MFI 12 result in the concentration values of  $\text{H}^+(\text{H}_2\text{O})_n$  varying from  $0.9 \text{ mol L}^{-1}$  to  $6.4 \text{ mol L}^{-1}$ . In the dehydration of CyOH under the first-order kinetic regime, we observed a volcano-shaped dependence of the TOFs on the ionic strength of zeolites at each temperature (Figure 2A, Supporting Information, Figure S6). The TOF increased at lower ionic strength until  $3 \text{ mol L}^{-1}$  and decreased again at higher ionic strength. Comparing the volcano rate dependence in the zeroth- and first-order kinetic regimes, the position for a maximum of TOF value was found at  $2\text{--}3 \text{ mol L}^{-1}$  for both cases. This similarity clearly reflects identical kinetic situations, independent of the coverage of sorbed substrates in zeolite micropores.

We conclude that the varying reaction rates are a consequence of the non-ideal thermodynamic states of all reactive substrates in the reaction path, which determines the transition free energies and in turn the overall catalytic activities (Supporting Information, Table S5). The reaction rates are, hence, required to be expressed as the functions of activities and activity coefficients.<sup>[11]</sup> H-MFI zeolite containing zero ionic strength in the pores was hereinafter referred to as an ideal condition. In fact, it was represented by the extremely diluted concentration of hydronium ions, because it was experimentally impossible to measure the reaction rate for zeolite H-MFI with zero BAS concentrations. The TOF(0), which denotes the TOF value under an ideal

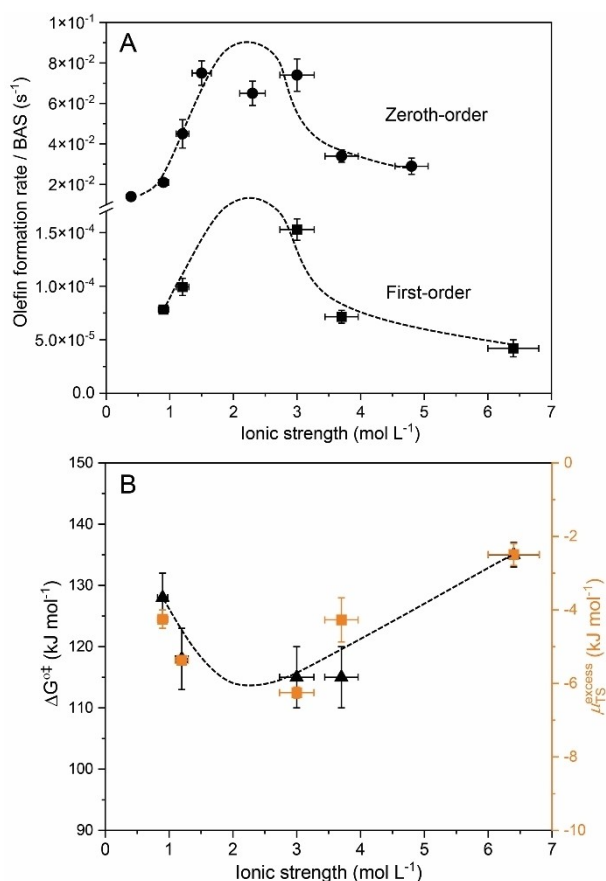


**Figure 2.** A) TOFs for H-MFI zeolite-catalyzed aqueous-phase cyclohexanol dehydration measured as a function of ionic strength in the first-order kinetic regime at 403 K. The data (circles) related to zeroth-order kinetics at 423 K are from ref. [6]. B) Reaction Gibbs free energy (triangles) and excess chemical potential (squares) of the transition state (TS) with varying ionic environments at 403 K. Dashed lines in both plots are to guide the eye.

condition, were therefore obtained by extrapolating the plots of TOF versus ionic strength to a zero ionic strength in first-order kinetic regimes. Under a non-ideal condition, in zeolite micropore abundant active sites stay un-occupied and the TOF(*I*) from Equation (4) (details of derivation see from the Supporting Information Note S3) is expressed in terms of the activity coefficient of the transition state ( $\gamma_{\ddagger}(I)$ ) and the TOF(0). Applying the transition state formula [Eq. (5)],  $\Delta G^{\ddagger}(\text{ideal})$ , the apparent Gibbs free energy of activation at an ideal state, is determined by the TOF(0).

$$\text{TOF}(I) = \frac{\text{TOF}(0)}{\gamma_{\ddagger}(I)} \quad (4)$$

$$\text{TOF}(0) = \frac{k_B T}{h} \exp\left(-\frac{\Delta G^{\ddagger}(\text{ideal})}{RT}\right) [\text{CyOH}] \quad (5)$$

where  $k_B$ ,  $h$ , and  $R$  are the Boltzmann constant, Plank constant and ideal gas constant, [CyOH] represents the concentration of CyOH in an aqueous phase.

The ionic environment of the zeolite pore influences the observed activation Gibbs free energy ( $\Delta G^{\ddagger}$ ) for the CyOH dehydration in the first-order kinetic regime through affecting the excess chemical potential of transition state ( $\mu_{\text{TS}}^{\text{excess}}$ ).<sup>[6]</sup> The  $\mu_{\text{TS}}^{\text{excess}}$  contributes to the activity coefficient of the transition state, which can also be restated as the functions of TOF (0) and TOF (*I*):

$$\mu_{\text{TS}}^{\text{excess}} = RT \ln \gamma_{\ddagger}(I) = RT \ln \frac{\text{TOF}(0)}{\text{TOF}(I)} \quad (6)$$

The values of  $\Delta G^{\ddagger}$  and  $\mu_{\text{TS}}^{\text{excess}}$  measured at 403 K are compiled in Figure 2B. Both the kinetic parameters show an inverse-volcano trend as a function of the ionic strength in zeolite micropores. A negative value of  $\mu_{\text{TS}}^{\text{excess}}$  points to the stabilization of the charged transition state by the ionic environment.<sup>[6]</sup> The largest extent of transition state stabilization is found at moderate ionic strength. Figure 3 displays the energy landscapes for aqueous-phase dehydration of CyOH on H-MFI zeolite that possesses hardly any ionic environment (ideal state, left part) and a high ionic strength (non-ideal state, right part). The values of  $\Delta G^{\ddagger}(I)$  are determined by all the changes in the transition state complexes and the excess interactions of adsorbed reactants/transition states with the confined hydronium ions in zeolite pores.<sup>[1e]</sup> The zeolite pores with zero ionic strength (considered as an ideal state), thus, do not induce excess chemical potential on reacting molecules. Therefore, for the catalytic reactions occurring in zeroth- and first-order kinetic regimes the excess Gibbs free energy ( $\Delta G_{\text{excess}}$ ) quantifies the difference between the free energy under a given ionic environment in zeolite ( $\Delta G^{\ddagger}(I)$ ) and that under an ideal condition ( $\Delta G^{\ddagger}(\text{ideal})$ ) [Eq. (7) and (8)]. This excess free energy reflects the impact from the ionic environment of microporous zeolites on the catalytic activities of a reaction.<sup>[6]</sup>

$$\Delta G_{\text{excess}}(0^{\text{th}}) = \Delta G_{0^{\text{th}}}^{\ddagger}(I) - \Delta G_{0^{\text{th}}}^{\ddagger}(\text{ideal}) \quad (7)$$

$$\Delta G_{\text{excess}}(1^{\text{st}}) = \Delta G_{1^{\text{st}}}^{\ddagger}(I) - \Delta G_{1^{\text{st}}}^{\ddagger}(\text{ideal}) \quad (8)$$

The  $\Delta G_{\text{excess}}$  also relates to the excess activation enthalpy ( $\Delta H_{\text{excess}}$ ) and entropy ( $\Delta S_{\text{excess}}$ ) ( $\Delta G_{\text{excess}} = \Delta H_{\text{excess}} - T\Delta S_{\text{excess}}$ ). The values of  $\Delta H_{\text{excess}}$  and  $\Delta S_{\text{excess}}$ , which are calculated to be negative for all the studied H-MFI zeolites, are plotted in Figure 4A by showing a linear correlation (that is, an enthalpy-entropy compensation effect).<sup>[12]</sup> Increasing ionic strength induces a stronger impact on  $\Delta S_{\text{excess}}$  by lowering the entropy gain, which is predominately linked with the formation and stabilization of charged transition state complexes in zeolite pores. In this case, it brings in also the beneficial enthalpic stabilization to overweigh the penalty of a lowering in entropy, endowing an enhancement of the rate for the catalytic CyOH dehydration on zeolites. CyOH dehydration with a maximum reaction rate manifests the values of  $\Delta H_{\text{excess}}$  and  $\Delta S_{\text{excess}}$  ranged in  $-35$ – $-25$  kJ mol<sup>-1</sup> and  $-70$ – $-50$  J mol<sup>-1</sup> K<sup>-1</sup>, respectively. A higher ionic strength (that is, the ionic environment after the position of maximum turnover rate) influences the activity gain by a means of increasing the

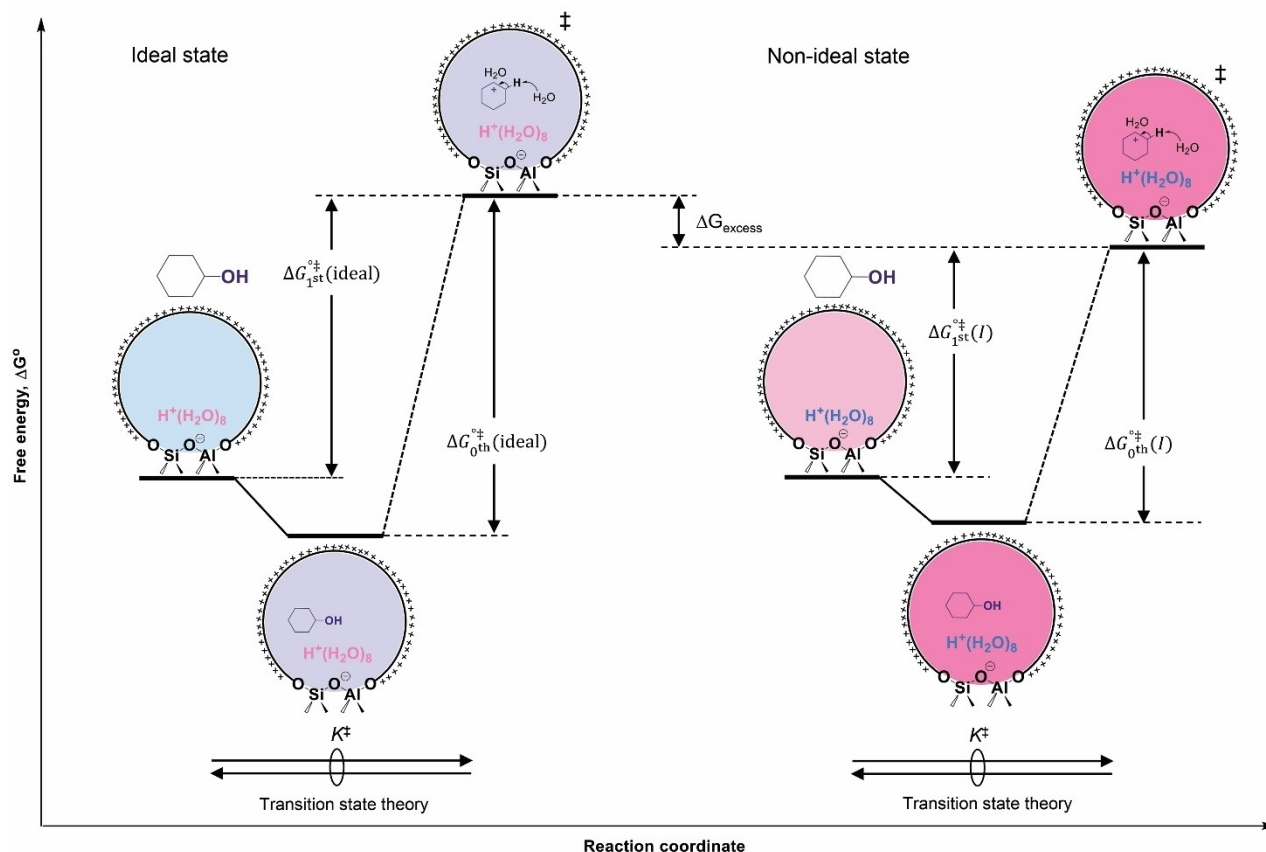


**Figure 3.** The illustration of the sequence of steps for the formation of transition states within zeolites under ideal state and non-ideal state condition. The combination of zeolite and CyOH in the aqueous phase was treated as the reference state for the formation of the transition states in the pores. The reference states are in equilibrium with the formation of transitions states, as described with the transition state equilibrium constant ( $K^\ddagger$ ). The sloping dashed lines indicate there are some elementary steps connecting in between two states.

enthalpic barrier, although there is a characteristic greater gain in  $\Delta S_{\text{excess}}$ . This phenomenon has also been observed from the alcohol dehydration in the zeroth-order kinetic regimes catalyzed by Brønsted acidic zeolites, of which the pores are fully filled with both substrate molecules (i.e., CyOH and substituted CyOH) and intraporous hydronium ions ( $\text{H}^+(\text{H}_2\text{O})_n$ ).<sup>[3,5]</sup>

As illustrated in Figure 4B, in the channel of H-MFI zeolite the distance of the center of hydronium ions is  $d_{\text{h-h}}$  and the boundary distance between two neighboring hydronium ions is  $d_{\text{b-b}}$ . The values of  $d_{\text{h-h}}$  and  $d_{\text{b-b}}$  decrease with the increasing of ionic strength in the zeolite micropores (Figure 4C). The CyOH adsorbs in the void space between two hydronium ions and, thus, the CyOH uptake shows a reduction with the increased ionic strength or the concentration of BAS sites (Scheme 1). Once the ionic strength in H-MFI micropores increase to a high value (i.e.,  $>3 \text{ mol L}^{-1}$ ), the average volume of the voids become less than the  $V_{\text{vdw}}$  value of CyOH. Under these conditions the work to be done to accommodate the transition state causes in the sum a gradually lower stabilization (and hence a higher entropy) of the transition state. Figure 4D shows this dependence in terms of activation enthalpy ( $\Delta H^{\ddagger}$ ) and entropy ( $\Delta S^{\ddagger}$ ) as a function of the distance  $d_{\text{b-b}}$  between

two neighboring  $\text{H}^+(\text{H}_2\text{O})_n$ . Both activation parameters reach the minimum positions at the  $d_{\text{b-b}}$  between 0.5 and 0.8 nm. The differences in  $\Delta H^{\ddagger}$  and  $\Delta S^{\ddagger}$  indicate the sensitivity of the transition states for CyOH dehydration to the ionic environments of zeolite and, thus, accounting for the volcano-shaped plot of catalytic turnover rates.

As a side note, the confined hydronium ions in H-MFI zeolite have been determined to possess a volume of  $(239 \pm 15) \text{ \AA}^3$ <sup>[2e]</sup> and the composition ( $\text{H}^+(\text{H}_2\text{O})_{7-8}$ ) is characteristically invariant with the temperature<sup>[6]</sup> and adsorbates (Supporting Information, Figure S2–S5). The number of CyOH molecules that the voids between two neighboring hydronium ions can accommodate are estimated by normalizing the void volume to the  $V_{\text{vdw}}$  of CyOH ( $193 \text{ \AA}^3$  at  $398 \text{ K}$ <sup>[14]</sup>). Based on a cylindrical model for the void space in H-MFI zeolite cavities ( $5.6 \times 5.4 \text{ \AA}$  in diameter), the volume of void could fall in a range allowing for the sorption of 0.8–1.0 number of CyOH, irrespective of the pore-filling degree of zeolite (Supporting Information, Table S6). The substrate to hydronium ion ratio is around 1:1 for the highest reaction rate in the zeroth-order kinetic regime,<sup>[6]</sup> where the adsorption of CyOH in zeolite is saturated. However, at first-order kinetic regime (i.e., 0.7 mM CyOH concentration), the maximum rate occurred at the CyOH to hydro-

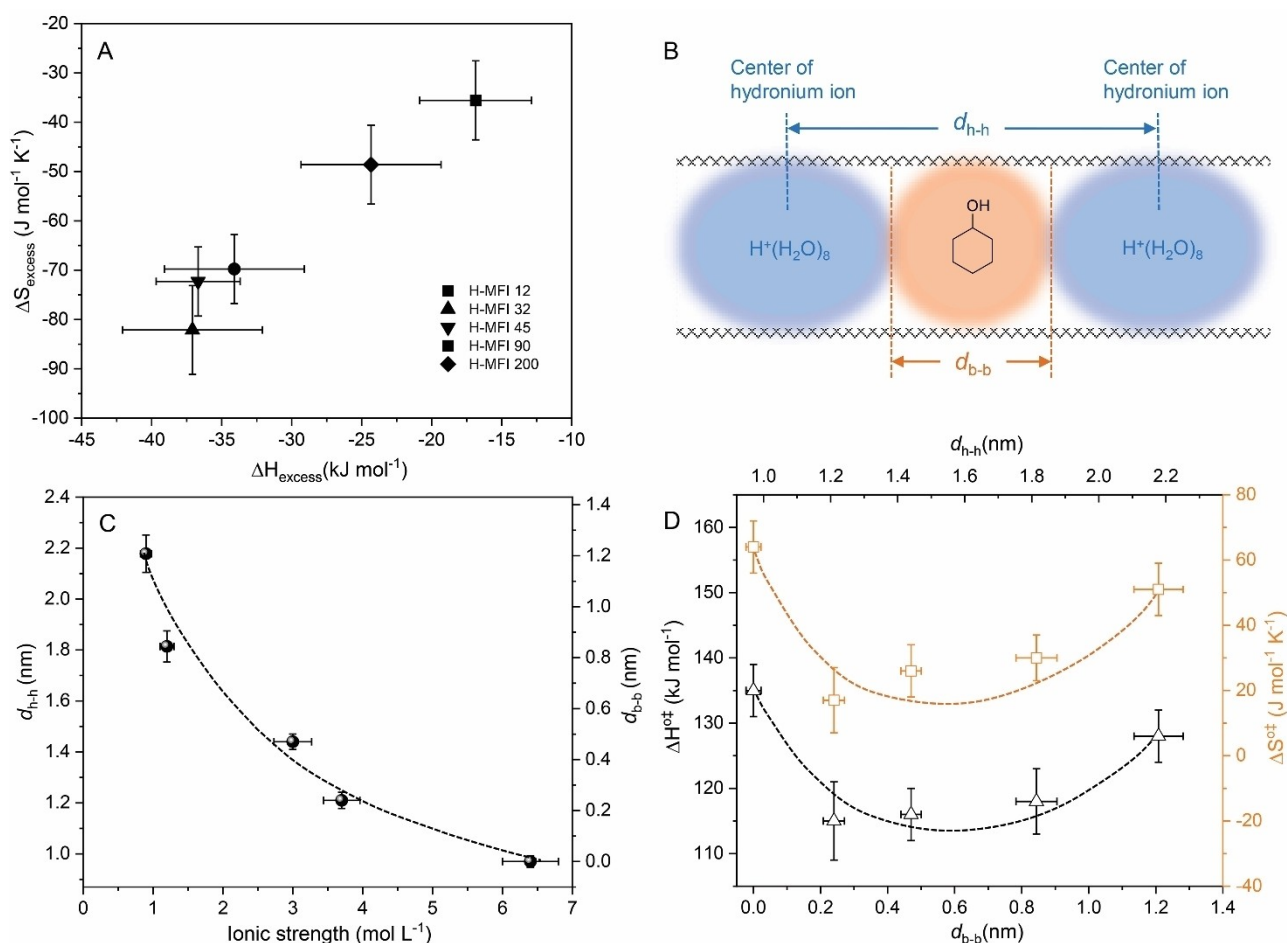


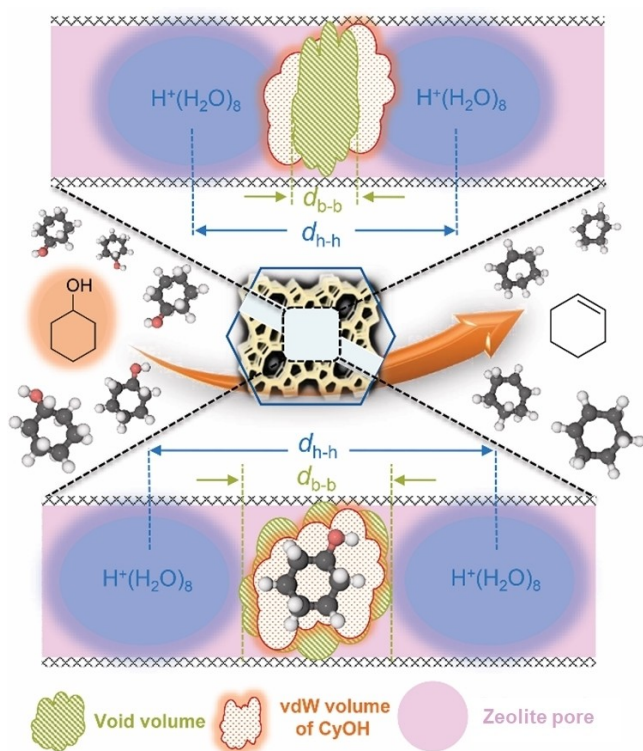
**Figure 4.** A) The relationship between the excess enthalpies ( $\Delta H_{\text{excess}}$ ) and excess entropies ( $\Delta S_{\text{excess}}$ ) induced by the ionic environment in H-MFI zeolites. B) Schematic illustration for the hydronium ions (blue color,  $\text{H}^+(\text{H}_2\text{O})_8$ ) in H-MFI channel. The mean distance of the center of two neighboring hydronium ions ( $d_{\text{h-h}}$ ) estimated by the cubic root of zeolite volume normalized to the number of hydronium ions.<sup>[2e,6]</sup> The boundary distance between two hydronium ions ( $d_{\text{b-b}}$ ) obtained by subtracting the length of hydronium ion from the  $d_{\text{h-h}}$ , assuming a cylindrical model for the hydronium ion in zeolite micropore.<sup>[13]</sup> The voids (orange color) between the two neighboring hydronium ions are the adsorption space for CyOH molecules. C) The calculated  $d_{\text{h-h}}$  and  $d_{\text{b-b}}$  with respect to the ionic strength in different zeolites. D) The activation enthalpy ( $\Delta H^{\ddagger}$ ) and entropy ( $\Delta S^{\ddagger}$ ) as a function of  $d_{\text{h-h}}$  and  $d_{\text{b-b}}$ . The surrounding solid lines on the symbols in (A), (C) and (D) plots are error bars. Dashed lines in (C) and (D) plots are to guide the eye.

nium ion ratio of ca. 0.1 (Supporting Information, Figure S7). This indicates that the apparent substrate to hydronium ion ratio in the zeolite micropore is not the criterion to determine catalytic reaction rate.

The ionic environment inside zeolite creates specific interactions with the  $\text{H}^+(\text{H}_2\text{O})_n$  and further influence the chemical potentials of reacting molecules. The enhanced reaction kinetics are a consequence of destabilizing the ground state (Supporting Information, Figure S8) and stabilizing the transition state by the  $\text{H}^+(\text{H}_2\text{O})_n$  under an ionic strength.<sup>[6]</sup> The positive effect is partly compensated at high ionic strength by the rearrangement required to stabilize the transition state, i.e., the partial rearrangement of the  $\text{H}^+(\text{H}_2\text{O})_n$ -zeolite (cation-anion) pairs. It should be noted that the larger size of the transition state of the carbenium ion compared to adsorbed CyOH or a lower concentration of the cyclohexyl oxonium ion are the physical reasons for the thermodynamic manifestation. The active sites required to

achieve a maximum turnover rate are quantified to be comprising of 1–2 hydronium ion clusters per unit cell (Supporting Information, Table S6), corresponding to an ionic strength range from 1.5 to 2.5  $\text{mol L}^{-1}$ , regardless of the intraporous alcohol concentration. In contrast, in an open aqueous solution (e.g., hydrochloric acid (HCl)) the CyOH dehydration rate increased monotonically with the ionic strength that was tuned by using lithium chloride (LiCl) (Supporting Information, Figure S9). The different behavior has its cause in the fact that the work to separate hydronium ions and rearrange them with the anions of the zeolite was replaced only by a small overall volume increase for open solvents.

It should be emphasized that influences of rearrangement of water structures occluded in microporous zeolites on the stability of surface intermediates and transition states have been extensively investigated for different catalytic reactions.<sup>[15]</sup> For instance, Bates and co-workers reported



**Scheme 1.** Zeolite-confined ionic environment intrinsically facilitates an optimized accommodation of reactant molecule in the voids created among the hydrated hydronium ions in the pores.

the formation of extended hydrogen-bonding networks in H-BEA zeolite pores at an increased water pressure and the further solvation of water-ethanol-clusters that eventually led to a severe inhibition for gas-phase ethanol dehydration.<sup>[15d]</sup> Ways of manipulating the reactivity of zeolite catalysis by water structures can be diverse, since the formation/stabilization of water structures on the active sites in the pores depends on the zeolite topologies,<sup>[1e,15d,16]</sup> pore polarities (i.e., hydrophilicity/hydrophobicity),<sup>[6,15]</sup> and the reaction conditions of interest (e.g., water pressure or water loadings).<sup>[17]</sup> Moreover, the kinetic phenomena related to the molecularly confined ionic environment of zeolite has been demonstrated cross the whole H-ZSM-5 zeolite crystals in our study. The ionic strength of the ionic environment can likely extend to other microporous materials and be applicable for explaining the impacts of water structures (e.g., water-alcohol-clustered hydronium ions,<sup>[15d]</sup> extended hydrogen-bonding water networks<sup>[15]</sup>) or other kinds of protonated clusters<sup>[18]</sup> on the kinetic relevance of catalysis at the solid-liquid interfaces.

## Conclusion

We show here that the microporous environment in zeolites leads to a maximum in impact of ionic strength on catalytic turnover rates by kinetically studying the intramolecular dehydration of CyOH in aqueous phase. Hydrated hydro-

num ions ( $\text{H}^+(\text{H}_2\text{O})_n$ ), derived from the hydration of zeolitic Brønsted acid sites by water molecules, are confined in zeolite micropores and comprise of one proton along with 7–8 water molecules. As cations, these hydronium ions together with zeolite framework anions generate a high ionic strength in zeolite micropores, a situation in which the organic reactant and the transition state behave non-ideally. In the hydronium ion-catalyzed alcohol dehydration via a carbenium ion transition state, the ionic environment destabilizes the adsorption ground state and enthalpically stabilizing the charged carbenium ion transition state, reducing the reaction free energy barrier and enhancing the catalytic reaction rates.

The rate increases monotonically with ionic strength in an open environment, i.e., aqueous HCl solution. However, it reaches a maximum and then drops at high ionic strength in zeolite pores. The maximum rate is a result of the optimized accommodation of reacting molecule and charged transition state by the confined pore space between two neighboring hydronium ions, and occurs when the space volume is close to the vdW volume of the substrate, regardless of the coverage or the pore-filling of the substrate. At high ionic strength, hydronium ions approach each other and the work to separate hydronium ions and rearrange them with the anions of the zeolite partly compensates the rate enhancement. In open aqueous phase, this work is replaced by a volume expansion towards the open solvents, thus, rates increase monotonically. The kinetic features of ionic environment in microporous zeolite demonstrated here can offer great opportunities for the design and optimization of optimal materials at an atomistic level.

## Acknowledgements

J.A.L. acknowledges the support by the U.S. Department of Energy (DOE), Office of Science, Office of Basic Energy Sciences (BES), Division of Chemical Sciences, Geosciences and Biosciences (Impact of catalytically active centers and their environment on rates and thermodynamic states along reaction paths, FWP 47319). Open Access funding enabled and organized by Projekt DEAL.

## Conflict of Interest

The authors declare no conflict of interest.

## Data Availability Statement

The data that support the findings of this study are available in the Supporting Information of this article.

**Keywords:** Alcohol Dehydration · Hydronium Ions · Ionic Environment · Kinetics · Zeolites

- [1] a) S.-M. Wu, X.-Y. Yang, C. Janiak, *Angew. Chem. Int. Ed.* **2019**, *58*, 12340–12354; *Angew. Chem.* **2019**, *131*, 12468–12482; b) J. W. Harris, J. S. Bates, B. C. Bukowski, J. Greeley, R. Gounder, *ACS Catal.* **2020**, *10*, 9476–9495; c) J. R. Di Iorio, B. A. Johnson, Y. Román-Leshkov, *J. Am. Chem. Soc.* **2020**, *142*, 19379–19392; d) K. Stanciakova, B. M. Weckhuysen, *Trends Chem.* **2021**, *3*, 456–468; e) D. T. Bregante, M. C. Chan, J. Z. Tan, E. Z. Ayla, C. P. Nicholas, D. Shukla, D. W. Flaherty, *Nat. Catal.* **2021**, *4*, 797–808.
- [2] a) L. Smith, A. K. Cheetham, R. E. Morris, L. Marchese, J. M. Thomas, P. A. Wright, J. Chen, *Science* **1996**, *271*, 799–802; b) A. Zecchina, F. Geobaldo, G. Spoto, S. Bordiga, G. Ricchiardi, R. Buzzoni, G. Petrini, *J. Phys. Chem.* **1996**, *100*, 16584–16599; c) A. Vjunov, J. L. Fulton, T. Huthwelker, S. Pin, D. Mei, G. K. Schenter, N. Govind, D. M. Camaioni, J. Z. Hu, J. A. Lercher, *J. Am. Chem. Soc.* **2014**, *136*, 8296–8306; d) A. Vjunov, M. A. Derewinski, J. L. Fulton, D. M. Camaioni, J. A. Lercher, *J. Am. Chem. Soc.* **2015**, *137*, 10374–10382; e) S. Eckstein, P. H. Hintermeier, R. Zhao, E. Baráth, H. Shi, Y. Liu, J. A. Lercher, *Angew. Chem. Int. Ed.* **2019**, *58*, 3450–3455; *Angew. Chem.* **2019**, *131*, 3488–3493; f) M. Wang, N. R. Jaegers, M.-S. Lee, C. Wan, J. Z. Hu, H. Shi, D. Mei, S. D. Burton, D. M. Camaioni, O. Y. Gutiérrez, V.-A. Glezakou, R. Rousseau, Y. Wang, J. A. Lercher, *J. Am. Chem. Soc.* **2019**, *141*, 3444–3455.
- [3] a) P. H. Hintermeier, S. Eckstein, D. Mei, M. V. Olarte, D. M. Camaioni, E. Baráth, J. A. Lercher, *ACS Catal.* **2017**, *7*, 7822–7829; b) L. Milakovic, P. H. Hintermeier, Q. Liu, H. Shi, Y. Liu, E. Baráth, J. A. Lercher, *J. Catal.* **2020**, *390*, 237–243; c) M. Shetty, H. Wang, F. Chen, N. Jaegers, Y. Liu, D. M. Camaioni, O. Y. Gutiérrez, J. A. Lercher, *Angew. Chem. Int. Ed.* **2021**, *60*, 2304–2311; *Angew. Chem.* **2021**, *133*, 2334–2341; d) L. Milaković, P. H. Hintermeier, Y. Liu, E. Baráth, J. A. Lercher, *Angew. Chem. Int. Ed.* **2021**, *60*, 24806–24810; *Angew. Chem.* **2021**, *133*, 25010–25014.
- [4] a) S. Eckstein, P. H. Hintermeier, M. V. Olarte, Y. Liu, E. Baráth, J. A. Lercher, *J. Catal.* **2017**, *352*, 329–336; b) Y. Liu, E. Baráth, H. Shi, J. Hu, D. M. Camaioni, J. A. Lercher, *Nat. Catal.* **2018**, *1*, 141–147.
- [5] a) Y. Liu, A. Vjunov, H. Shi, S. Eckstein, D. Camaioni, D. Mei, E. Baráth, J. A. Lercher, *Nat. Commun.* **2017**, *8*, 14113; b) H. Shi, S. Eckstein, A. Vjunov, D. M. Camaioni, J. A. Lercher, *Nat. Commun.* **2017**, *8*, 15442.
- [6] N. Pfriem, P. H. Hintermeier, S. Eckstein, S. Kim, Q. Liu, H. Shi, L. Milakovic, Y. Liu, G. L. Haller, E. Baráth, Y. Liu, J. A. Lercher, *Science* **2021**, *372*, 952–957.
- [7] a) N. Y. Chen, W. E. Garwood, *Catal. Rev. Sci. Eng.* **1986**, *28*, 185–264; b) T. F. Degnan, *J. Catal.* **2003**, *216*, 32–46.
- [8] a) H. S. Fogler, *Elements of Chemical Reaction Engineering*, Prentice-Hall, Englewood Cliffs, **1986**; b) C. Ercan, F. M. Dautzenberg, C. Y. Yeh, H. E. Barner, *Ind. Eng. Chem. Res.* **1998**, *37*, 1724–1728; c) W. Fu, L. Zhang, D. Wu, M. Xiang, Q. Zhuo, K. Huang, Z. Tao, T. Tang, *J. Catal.* **2015**, *330*, 423–433.
- [9] D. D. Do, *Adsorption Analysis: Equilibria and Kinetics, Vol. 2*, Imperial College Press, London, **1998**, pp. 149–190.
- [10] a) K. Zhang, R. P. Lively, J. D. Noel, M. E. Dose, B. A. McCool, R. R. Chance, W. J. Koros, *Langmuir* **2012**, *28*, 8664–8673; b) M. Van den Bergh, A. Krajnc, S. Voorspoels, S. R. Tavares, S. Mullens, I. Beurroies, G. Maurin, G. Mali, D. E. De Vos, *Angew. Chem. Int. Ed.* **2020**, *59*, 14086–14090; *Angew. Chem.* **2020**, *132*, 14190–14194.
- [11] R. J. Madon, E. Iglesia, *J. Mol. Catal. A* **2000**, *163*, 189–204.
- [12] a) E. Cremer, *Adv. Catal.* **1955**, *7*, 75–91; b) D. W. Flaherty, E. Iglesia, *J. Am. Chem. Soc.* **2013**, *135*, 18586–18599.
- [13] a) D. H. Olson, G. T. Kokotailo, S. L. Lawton, W. M. Meier, *J. Phys. Chem.* **1981**, *85*, 2238–2243; b) A. Saito, H. C. Foley, *AIChE J.* **1991**, *37*, 429–436.
- [14] W. V. Steele, R. D. Chirico, S. E. Knipmeyer, A. Nguyen, *J. Chem. Eng. Data* **1997**, *42*, 1021–1036.
- [15] a) M. J. Cordon, J. W. Harris, J. C. Vega-Vila, J. S. Bates, S. Kaur, M. Gupta, M. E. Witzke, E. C. Wegener, J. T. Miller, D. W. Flaherty, D. D. Hibbitts, R. Gounder, *J. Am. Chem. Soc.* **2018**, *140*, 14244–14266; b) D. T. Bregante, A. M. Johnson, A. Y. Patel, E. Z. Ayla, M. J. Cordon, B. C. Bukowski, J. Greeley, R. Gounder, D. W. Flaherty, *J. Am. Chem. Soc.* **2019**, *141*, 7302–7319; c) D. T. Bregante, D. W. Flaherty, *ACS Catal.* **2019**, *9*, 10951–10962; d) J. S. Bates, B. C. Bukowski, J. Greeley, R. Gounder, *Chem. Sci.* **2020**, *11*, 7102–7122; e) J. S. Bates, R. Gounder, *Chem. Sci.* **2021**, *12*, 4699–4708.
- [16] E. Grifoni, G. M. Piccini, J. A. Lercher, V.-A. Glezakou, R. Rousseau, M. Parrinello, *Nat. Commun.* **2021**, *12*, 2630.
- [17] a) Y. Zhi, H. Shi, L. Mu, Y. Liu, D. Mei, D. M. Camaioni, J. A. Lercher, *J. Am. Chem. Soc.* **2015**, *137*, 15781–15794; b) D. Mei, J. A. Lercher, *AIChE J.* **2017**, *63*, 172–184.
- [18] a) J. R. Di Iorio, A. J. Hoffman, C. T. Nimlos, S. Nystrom, D. Hibbitts, R. Gounder, *J. Catal.* **2019**, *380*, 161–177; b) J. S. Bates, R. Gounder, *J. Catal.* **2020**, *390*, 178–183.

Manuscript received: June 13, 2022

Accepted manuscript online: November 1, 2022

Version of record online: December 8, 2022